I.A.U. Karaj Branch

Journal of Applied Chemical Research, 11, 1, 135-149 (2017)

Journal of Applied Chemical Research
www.jacr.kiau.ac.ir

Kinetic Study and Equilibrium Isotherm Analysis of Nickel (II) Adsorption onto Alginate-SBA-15 Nanocomposite

Mohammadreza Kosari[1], Hamid Sepehrian[2*], Javad Fasihi[2], Masoud Arabieh[2]

[1]Department of Energy Engineering, Sharif University of Technology, Tehran, Iran

[2]Nuclear Science and Technology Research Institute, Tehran, Iran

(Received 09 Jul. 2016; Final version received 25 Sep. 2016)

Abstract

The present work was undertaken to evaluate the feasibility of nickel (II) removal from aqueous solution by adsorption onto a biopolymer adsorbent. The adsorbent was prepared using modification of mesoporous silicate SBA-15 with alginate biopolymer (alginate-SBA-15) by encapsulation method. Morphological structure of the obtained nanocomposite adsorbent was characterized by XRD, scanning electron microscopy, nitrogen porosimetry technique, and fourier transform infrared spectroscopy. Batch adsorption experiments were carried out to investigate influence of operational parameters such as pH, contact time and initial concentration on alginate-SBA-15 adsorption behavior. Kinetics study revealed that the pseudo-second-order model provided well mathematical description of the experimental data. Out of several isotherm models, the Langmuir, Ferundlich, Dubinin-Radushkevich, Redlich-Peterson, and Temkin models were applied to adsorption data to estimate adsorption capacity. The equilibrium adsorption data are well modeled by the Langmuir isotherm than the others and the maximum adsorption capacity found to be 58.82 mg g^{-1}.

Keywords: *Mesoporous SBA-15, Alginate, Nanocomposite, Biopolymer sorbent, Nickel (II), Adsorption.*

Nomenclature

C_i Initial concentration of nickel ions (mg l^{-1});

C_f Final concentration of nickel ions (mg l^{-1});

V Volume of nickel solution (ml) ;

m Mass of adsorbent (g) ;

q Adsorption capacity of the adsorbent (mg g^{-1});

q_e Amount of nickel ions adsorbed per unit weight of the sorbent (mg g^{-1}) ;

***Corresponding author:** Hamid Sepehrian, Nuclear Science and Technology Research Institute, P.O. Box 143995113, Tehran, Iran. E-mail: hsepehrian@aeoi.org.ir.*

q_{max} Maximum adsorption capacity (mg g^{-1});
C_e Equilibrium concentration of the nickel (II) in solution (mmol l^{-1}) ;
kl Langmuir isotherm constant (l $mmol^{-1}$) ;
n Freundlich constants corresponded to the adsorption intensity;
k_f Freundlich constants corresponded to the adsorption capacity;
q_t Amount of nickel adsorbed (mg g^{-1}) on adsorbent at time t;
K_1 Pseudo first-order rate constant of adsorption (l min^{-1}) ;
K_2 Pseudo second-order rate constant of adsorption (g mg^{-1} min^{-1}) ;
K_R Redlich-Peterson isotherm constant (l g^{-1});
α^R Redlich-Peterson isotherm constant (l $mmol^{-1}$);
β_R Redlich-Peterson isotherm exponent;
β_D Dubinin-Radushkevich isotherm constant (porosity factor) (mol2 KJ^{-2});
ε Polanyi potential;
q_m Monolayer adsorption capacity;
R Universal gas constant (8.314 J mol 1 $\circ K^{-1}$);
T Absolute temperature (K);
K_T Temkin isotherm constant (dm3 $mmol^{-1}$);
A_T Temkin adsorption energy change between two neighboring adsorption sites (J $mmol^{-1}$);

Introduction

Nickel environmental contamination can regularly result of different natural and industrial processes such as mining and metallurgy of nickel, chemical and food processing industries, especially as catalysts and pigments[1, 2]. Due to extravagant consumption,the readily spreading of nickel in environment and production rate has been of major concern because of the high risk to humans, plants and groundwaters. Such materials (i.e. heavy metal ions), unlike organic pollutants, after releasing into environment do not undergo biodegradation and incline to persist indefinitely, circulating and finally amassing through the food chain[3]. As well as significant impact of heavy metals on the environment, interference of heavy metal ions with functional groups of essential enzymes even at low concentrations has been well established [1, 4]. Different physical and chemical treatment methods for removal of nickel from aqueous solutions such as solvent extraction, electrochemical treatment, ion exchange, chemical precipitation, chemical oxidation/reduction, filtration, reverse osmosis, membrane technologies and evaporation recovery have been developed [5]. However, these methods for removal of nickel are inefficient because of their high costs, technical problems, and production of toxic chemical sludges.

In recent years, adsorption has drawn more attention toward the removal of heavy metals. Most of researchers who work on this area have employed various synthesized and natural adsorbent to reach the highest adsorption of heavy metal ions. However, most

of them are still following to synthesize new adsorbents, which have great advantages such as maximum adsorption capacity, low cost and regeneration ability. For example, sphagnum moss peat [6], microspora and lemna minor [7], crab shell particles [8] and multi-walled carbon nanotubes [9] are a few kinds of these adsorbents.

Alginate, a linear copolymer of a-L-guluronate (G) and a-D-mannuronate (M), is extendedly utilized as sorbent to remove heavy metal ions [10-12]. Alginate, created of many chains, forms electronegative cavities enable it to hold the cations via ionic interactions. As a result, cross-linking and substitution of heavy ions with these cavities makes the alginate an ideal template from view of adsorption. On the other hand, nanoporous materials because of their large surface area and the attributed pore size were regularly used in the removal of heavy metals. Meanwhile, becauseall of these materials like nanosilica SBA-15have ultrafine structure's disadvantage, this means that handling a treatment operation with such adsorbents will encounter with some problems such as filtration of solids from liquid during the sorption process.

The current study is aimed at developing an adsorbent, which is the combination of alginate and SBA-15 (alginate-SBA-15), by encapsulation method. This method modifies the structure of SBA-15 and converts it to an adsorbent with a normalized structure. Subsequently, morphological structure of the obtained adsorbent is characterized by XRD, SEM, nitrogen adsorption-desorption and FTIR spectroscopy. In the last part, the effects of operational parameters such as pH, initial concentration of nickel and contact time are also investigated through batch experiments.

Experimental

Materials

Stock solution of nickel (II) ions (1000 ppm) was prepared by dissolving appropriate amount of nickel (II) nitrate, $Ni(NO_3)_2.6H_2O$, in distilled water. Pluronic P123 triblock and sodium alginate used in the current study were purchased from Sigma-Aldrich (Milwaukee, WI, USA). All other mineral reagents were of analytical grade from Merck (Darmstadt, Germany).

Preparation of alginate-SBA-15

Nanoporous silica SBA-15 has been prepared according to our previous work [13]. In a typically procedure, 4 g of pluronic P123 triblock copolymer surfactant (EO_{20}-PO_{70}-EO_{20}) is dissolved in water/HCl solution 2M and then TEOS is added. Subsequently the mixtureis stirred for 8 h and then aged for 24 h at room temperature. After filtering, washing and rinsing, calcination was performed at 550 °C for 6 h to remove residual organic component (i.e. triblock copolymer). Alginate-SBA-15 nanocompositewas prepared by

mixing the sonicated suspension of SBA-15 (13% w/w) with 100 ml solution containing 1.5% Na-alginate. The resulting solution, after situating just under agitation using a high speed disperser for about 2 h, was introduced into 0.1 M $Ca(NO_3)_2$ solution through a 0.3 mm medical needle. Under this condition, gel type spherical beadswere formed and their sizes adjusted using a pneumatic cutter acting through setting a controllable air flow around the injecting needle. In order to strengthen the formed nanocomposite, it was restirred in 0.1 M $Ca(NO_3)_2$ solution for 3 h, and after three times washing with pure water it was dried at 40 °C for 10 h. Before the adsorption experiment, the weight ratio of Na-alginate and SBA-15 before the mixing stage had obtained. So, the amount of SBA-15 was recorded 50% in composite. The granules of calcium alginate finally prepared in a similar way with addition of sodium alginate into calcium nitrate solution.

Alginate-SBA-15 characterization

The alginate-SBA-15 nanocomposite was characterized by X-ray diffraction (XRD), scanning electron microscopy (SEM), and nitrogen porosimetry techniques. XRD analysis of samples were carried out with a Philips X'pert powder diffractometer system with Cu-Kα (λ=1.541 Å) radiation from 1.5° to 10° (2θ) at a scan rate of 0.02° (2θ). The nitrogen adsorption-desorption tests were conducted at 77 K using Quantachrome NOVA 2200e. FTIR spectra were recorded using a Bruker FTIR spectrophotometer model Vector-22 over the wave number range of 4000-400 cm^{-1}. A LEO 1455VP scanning electron microscopy was also used for surface morphology study. Quantitative determination of the nickel ion was carried out using an inductively coupled plasma (ICP) Varian turbo model 150-Axial Liberty.

Batch adsorption experiments

Equilibrium batch adsorption tests were carried out to investigate adsorption behavior of alginate-SBA-15 for removal of nickel form aqueous solution. In this method, 10 mg of adsorbent were introduced in 10 ml of Ni(II) stock solution whose its initial concentration was adjusted on a desire value. After a given time of suspension shaking and attaining equilibrium, adsorbent was separated from solution by filtration. Nickel concentration of the aqueous-phase was measured using an ICP. The adsorption capacity of adsorbent was calculated by below equation (Eq. 1):

$$q(mg\ g^{-1})=\left(C_i-C_f\right)*\frac{V}{m} \qquad (1)$$

In order to kinetic study, pseudo first-order and pseudo second-order kinetic models were applied on experimental resultsto describe the adsorption rate. These kinetic models are expressed as follows (Eq. 2 and 3):

Pseudo first-order model [14]

$$\log\left(\frac{q_e}{q_e\text{-}q_t}\right)=\left(\frac{K_1}{2.303}\right)t \qquad (2)$$

Pseudo second-order model [14]

$$\frac{t}{q_t}=\frac{1}{K_2q_e^{\,2}}=\frac{t}{q_e} \qquad (3)$$

where K_1(L min^{-1}) and K_2 (g mg^{-1} min^{-1}) stand for the rate constant of adsorption. Values of K_1 and K_2 were calculated from the straight line graph of $\log(q_e–q_t)$ versus t and (t/q_t) versus t for different initial concentrations of the nickel (II) ion, respectively.

For revealing the relationship of the amount of Ni(II) ions between the aqueous and solid phase, isotherm study was performed. Out of several isotherms, the Langmuir, Freundlich, Redlich-Peterson, Dubinin-Radushkevich, and Temkin isotherms were applied on the nickel (II) adsorption data. The isotherm models are represented in Table 1.

Table 1. Isotherm models and their linear forms

Isotherm model		Linear form	Plot	Ref.
Langmuir	$q_e=\frac{q_{max}k_lC_e}{1+k_lC_e}$ (4)	$\frac{C_e}{q_e}=\frac{1}{q_{max}k_l}+\frac{C_e}{q_{max}}$ (5)	$\frac{C_e}{q_e}$ vs. C_e	[15]
Freundlich	$q_e=k_fC_e^{\,1/n}$ (6)	$\log q_e=\log k_f+\frac{1}{n}\log C_e$ (7)	$\log q_e$ vs. $\log C_e$	[15]
Dubinin-Radushkevich (D-R)	$\frac{q_e}{q_m}=\exp(-\beta_D\varepsilon^2)$ (8)	$\ln(q_e)=\ln(q_m)-\beta_D\varepsilon^2$ (9) $\varepsilon=RT\ln\left[1+(\frac{1}{C_e})\right]$(10)	$\ln q_e$ vs. ε^2	[16]
Redlich-Peterson (R-P)	$q_e=\frac{K_RC_e}{1+\alpha_RC_e^{\beta_R}}$ (11)	$\ln\left(\left(\frac{K_RC_e}{q_e}\right)\text{-}1\right)=\beta_R\ln(C_e)+\ln(\alpha_R)$ (12)	$\ln\left(\frac{K_RC_e}{q_e}\right)$ vs. $\ln(C_e)$	[16]
Temkin	$q_e=\frac{RT}{A_T}\ln(K_TC_e)$ (13)	$q_e=\frac{RT}{A_T}[\ln(K_T)+\ln(C_e)]$ (14)	q_e vs. $\ln C_e$	[16]

The Langmuir isotherm model (Eq. 4) is based on monolayer metal ion sorption on the adsorbent surface with specific homogenous sites. The linearized form of the Langmuir model (Eq. 5) is used to make plotting and evaluation of model parameters and sorption capacity. The Freundlich isotherm model (Eq. 6) assumes that enthalpy of adsorption is independent of the amount adsorbed and heterogeneous surface is involved in the sorption process. This model can be rearranged in a logarithmic form (Eq. 7) in order to determination of the Freundlich parameters. As a more general equation than Langmuir model, Dubinin–Radushkevich (D-R) isotherm (Eq. 8) does not assume a homogenous surface with energetically equivalent sorption sites. The Dubinin–Radushkevich (D-R) isotherm was used to

determine the nature of the adsorption process viz. physisorption or chemisorptions[16]. Equation 9 represents the linear model of this equation. ε is the Polanyi potential relates to the adsorption potential theory presented by Polanyi-Dubinin suggensting the adsorption proceeds in the volume of adsorbent micropores as opposed to layer-by-layer adsorption or micropore walls[16], which it can be calculate using Eq. 10.

The Redlich-Peterson (R-P) equation (Eq. 11) is a consolidation of both Langmuir and Freundlich isotherms, in which it reaches the Langmuir model at lower concentration and converges to Freundlich equation at higher concentration of adsorbate. The Temkin isotherm model (Eq. 13) assumes that the fall in the heat of sorption is linear rather than logarithmic, as implied in Freundlich equation[17]. Equation 14 is the linear form of Temkin model, which it can be utilized for evaluation of isotherm constants.

Results and discussion

Characterization

XRD patterns of the SBA-15, alginate-SBA-15 nanocomposite and Ca-alginate are shown in Figure 1a. SBA-15 and alginate-SBA-15 nanocomposite show an intensify peak at 2θ smaller than 2°, along with some small peaks. Under such condition, it confirmed that mesoporous SBA-15 was formed and SBA-15 was orderly maintained in alginate-SBA-15 matrix.

Figure 1b represents FTIR spectra of the SBA-15, alginate-SBA-15 nanocomposite and Ca-alginate. FTIR spectrum of alginate-SBA-15 nanocomposite shows adsorption bands at 3450 cm^{-1} (OH stretching), 2900 cm^{-1} (CH stretching), 1610 cm^{-1} (COO-asymmetric stretching), and 1429 cm^{-1} (COO- symmetric stretching). The bands at 1125 cm^{-1} are due to the CO stretching of ether groups and the bands at 1065 cm^{-1} are related to carbon-oxygen stretching of alcohol group [18,19]. This reveals that all effective functional groups for nickel adsorption on SBA-15 and alginate are still present on alginate-SBA-15 even after encapsulation process and are available for interaction with nickel ions.

Figure1c illustrates the nitrogen adsorption isotherms of SBA-15, alginate-SBA-15 nanocomposite and Ca-alginate nanocomposite. According to the SBA-15 and alginate-SBA-15 profile, it can be figured out that an assemblage of non-intersecting tubular pores was happened. This case, typical adsorption profile of type IV, is generally associated with mesoporous adsorbents[20]. Sinceadsorption profile was of type IV (i.e. the mesopore volume is obtained by assuming the condensate density to be that of liquid nitrogen), thus the aforementioned about formation of mesoporous SBA-15 and the presence of mesoporous SBA-15 in the alginate-SBA-15 matrix is accurate.

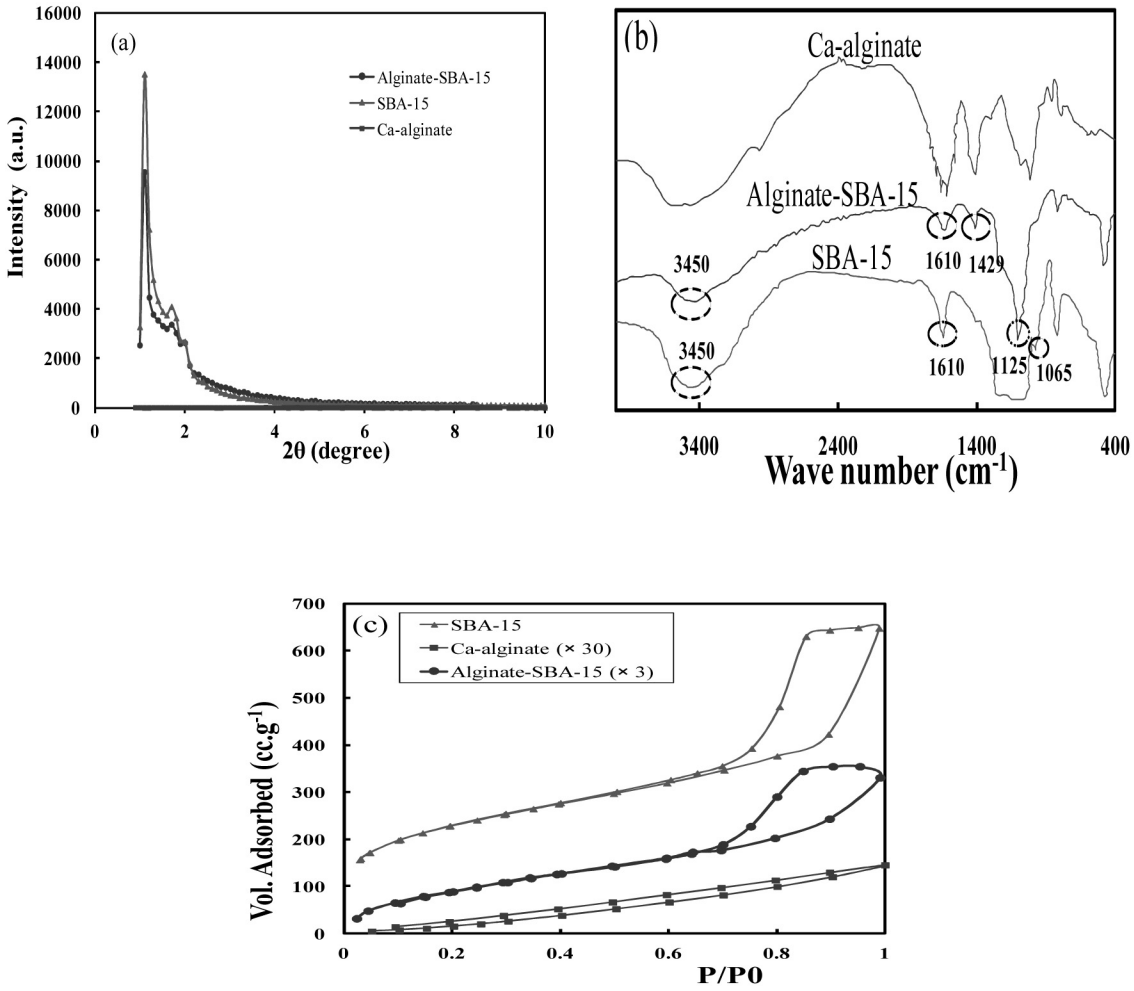

Figure 1. (a) XRD patterns; (b) FTIR spectra; (c) Nitrogen adsorption/desorption isotherms of the Ca-alginate, SBA-15 and alginate-SBA-15[13].

Surface area, pore volume and pore diameter values were presented in Table 2. Among the three components, the SBA-15 possesses high surface area and pore volume than alginate-SBA-15. Similar attribute can be observed in the pore diameter of SBA-15 and alginate-SBA-15 nanocomposite. This condensation effect may be due to the polymerization of monomers inside the channels of SBA-15 as a result of encapsulation method.

Table 2. Morphological properties of Ca-ALG, SBA-15 and alginate-SBA-15.

Sample	Pore volume ($cm^3\ g^{-1}$)	Surface area ($m^2\ g^{-1}$)	Pore diameter (nm)
CaALG	0.009	3.8	2.29
SBA-15	0.74	749	12.6
alginate-SBA-15	0.17	122	9.7

SEM images of the surface of SBA-15 and alginate-SBA-15 nanocomposite represented in Figures 2a & 2b, display a non-uniform wavy and rough structure on surface with some ripples along with lateral dimensions. Under such condition, effective area increased. A glimpse at the SEM micrograph of SBA-15 (Figure. 2a) discloses the presence of many pores with deep capillary, whereas alginate-SBA-15 nanocomposite has not porosity like SBA-15. This can be a result of immediate condensation during encapsulation process in which capillary obstruction and pore removing occurs due to the immobilization.

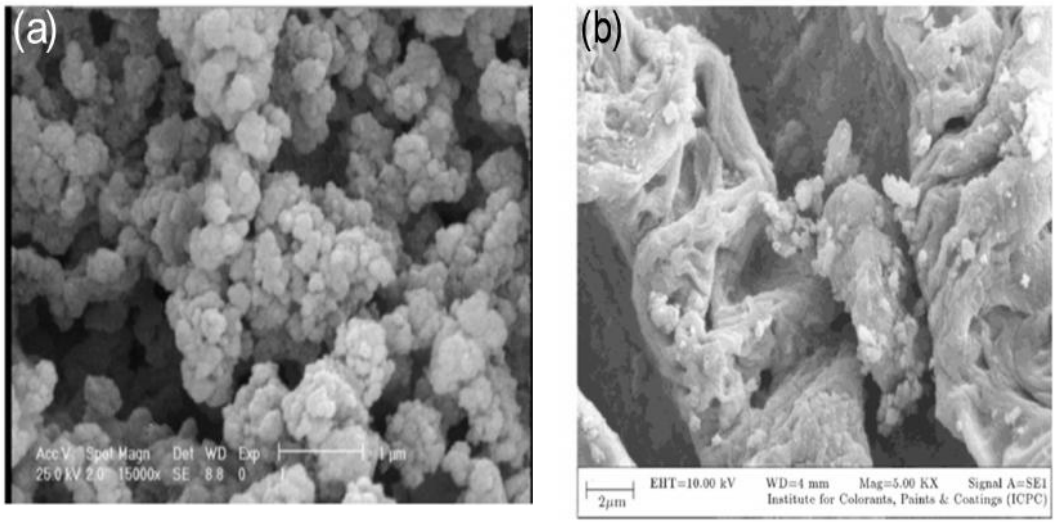

Figure2. (a) SEM image of SBA-15; (b) surface morphologies of alginate-SBA-15[13].

Effect of pH

The pH is the most effective parameter in the adsorption process. The adsorption rate and capacity strongly are the pH-dependent parameters. The effect of increasing pH on the adsorption behavior of alginate-SBA-15 nanocomposite was presented in Figure 3. It was observed that adsorption rate increases as the pH increased, so that nickel(II) adsorption leveled-up from pH 2 to 5 and then remained constant at around pH 5-7. This behavior may be discussed on the basis of the chemical interaction of nickel ions with functional groups on the adsorbent surface. The carboxylic functional groups deprotonation rate increased by increasing the pH and it may be cause of the increased binding between nickel ions and adsorbent sites. At lower pH, the protons of COOH functional groups cannot be easily separated, thereby, the possibility of binding to nickel ions reduced. In addition, the presence of many hydronium ions (H_3O^+) at lower pH closely associated with low adsorption of nickel (II) ions due to competing of the hydronium ions with nickel (II) ions for binding sites. On the other

hand, activation of electronegative cavities of alginate for holding nickel ions at higher pHs may be other synergetic effect in increasing sorption performance.

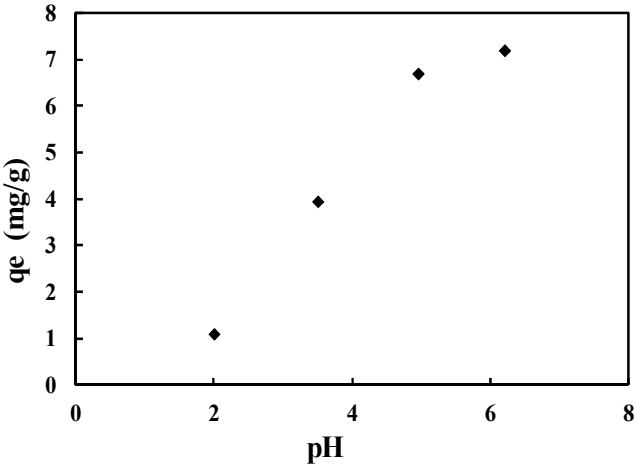

Figure 3. Effect of pH on nickel ions removal by alginate-SBA-15 nanocomposite, conditions: initial concentration=100 mg L^{-1} , $m_{alginate\text{-}SBA\text{-}15}$=10 mg, V_{Ni}=10 ml, T= 25 °C.

Kinetic study

To understand the relation between the contact time and adsorption behavior of alginate-SBA-15 nanocomposite, equilibrium concentration of nickel (II) ions were measured at different time intervals up to 5 h.

As can be seen in Figure 4a, the amount of adsorbed nickel (II) ions per weight of alginate-SBA-15 nanocomposite increased with time and equilibrium condition was achieved after 2.5 h. The resultswereused for kinetic study of nickel (II) removal from aqueous solution on alginate-SBA-15 nanocomposite. In order to investigate the governing mechanism on nickel sorption, the kinetic constants for nickel adsorption were determined by applying the pseudo first-order and pseudo second-order kinetic models. The upshot resultsof pseudo second order kinetic model weresketched in Figure 4b.

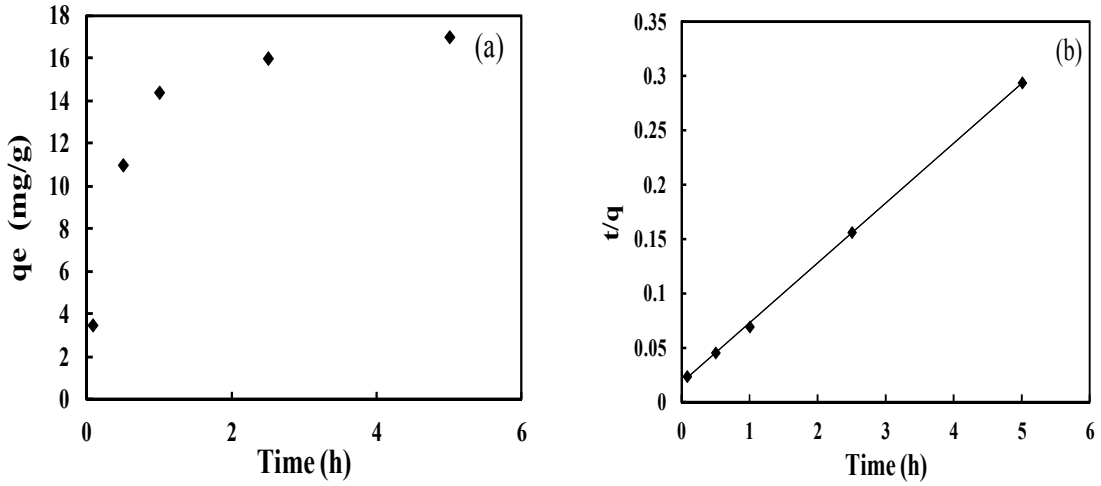

Figure 4. (a) Effect of contact time on Ni(II) adsorption performance of alginate-SBA-15 nanocomposite (Initial concentration: 100 mg L^{-1}) ; (b) Linearized experimental data of pseudo second order kinetic model curve.

The kinetics constants of pseudo first-order and pseudo second-order equations are presentedin Table 3. An examination of results show that pseudo second-order model has a better match with the adsorption of nickel on the alginate-SBA-15 nanocomposite results such as shown in Figure 4b.The confirmation of pseudo-second-order kineticsindicates that the concentrations of both adsorbate(nickel ions) and adsorbent (alginate-SBA-15) areinvolved in the rate determining step of the adsorptionprocess.

Table 3. Kinetics parameters for Ni(II) removal using alginate-SBA-15 nanocomposit.

Pseudo first-order			Pseudo second-order		
k_1(min^{-1})	q_e (mg g^{-1})	R^2	k_2(g mg^{-1} min^{-1})	q_e(mg g^{-1})	R^2
0.9792	10.76	0.915	0.1767	18.083	0.999

Adsorption isotherm

Figure 5a shows the isotherm adsorption graph of the nickel (II) uptake onto alginate-SBA-15. It can be seen that adsorption efficiency increased with increasing at initial concentration of nickel (II) ions. Based on Figure5b, Langmuir constants can be calculated from the trend line equation. According to the Freundlich model, by plotting of log q_e versus log C_e (Figure 5c), the values of K_f and n can be calculated from the intercept and slope, respectively. Comparison between Langmuir and Freundlich isotherm show that Langmuir model can better fit experimental data. It can be a result of homogenous distribution of active sites on the alginate-SBA-15 surface. Therefore, the adsorption process can be described by the formation of monolayer coverage of the Ni (II) ion on the homogenous adsorbent surface.

The linearized plot of Dubinin-Radushkevich isotherm model is represented in Figure6a. As

seen, the values of **β** and q_m can be determined using the slope and intercept of ln q_e versus ε^2 plot. According to q_m value, there is good agreement between the predicted sorption capacity by Langmuir model and D-R equation. In order to evaluation of the R-P isotherm model, plot of ln($K_R C_e/q_e$) versus ln (C_e) is sketched (see Figure 6b). The amounts of K_R, α_R, and β_R were solved in Microsoft Excel using R-P equation by minimizing the sum of square of the errors between the theoretical values for qe predicted by Eq. (11) and experimental ones. The magnitude of βR, which exist between 0 and 1 is utilized to characterize the isotherm in which; if β_R= 1, the Langmuir will be preferable isotherm, whereas if β_R= 0, the Freundlich isotherm will be the desirable one[16]. As shown in Table 4, calculated value of βR indicates that Langmuir model is the predominant isotherm model, which such argument was earlier resulted.

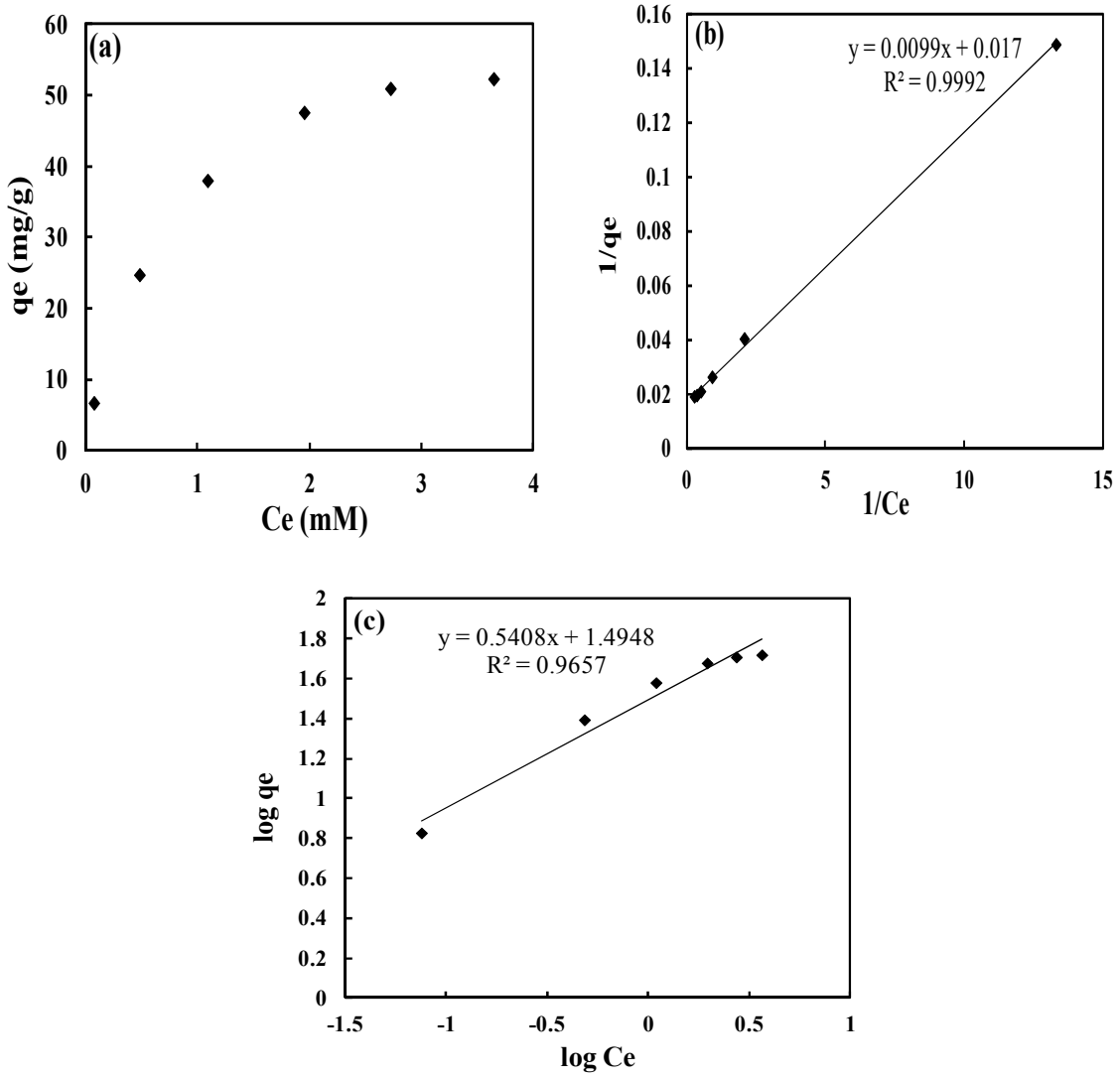

Figure 5. (a) Effect of initial concentration on the nickel (II) ion removal by alginate-SBA-15 nanocomposite; (b) Langmuir isotherm plot; (c) Freundlich isotherm plot.

The linearized plot of Temkin isotherm by plotting qe versus ln (C_e) was illustrated in Figure6c, in which the slope and intercept of resulted curve leads to determination of K_T and A_T values. However, all isotherm models are capable of representing the data satisfactorily, the isotherm parameters given in Table 4 show good agreement between the experimental data and the Langmuir isotherm results. Thus, the description of adsorption process can be related to the formation of monolayer coverage of the adsorbate on the homogenous adsorbent surface. The maximum adsorption capacity (q_{max}) of the alginate-SBA-15 nanocomposite was calculated as 58.82 mg g^{-1}.

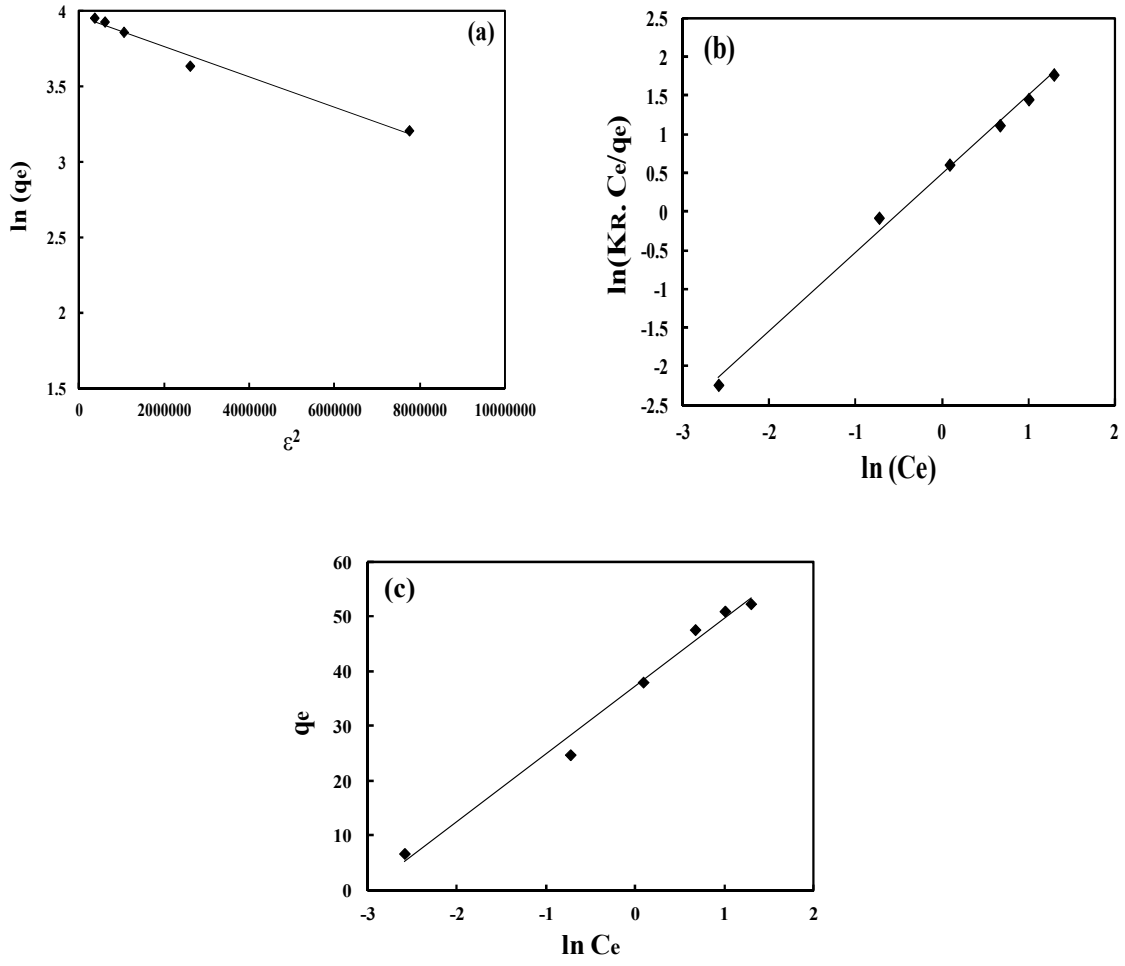

Figure 6. Plots of (a) Dubinin-Radushkevich (D-R), (b) Redlich-Peterson (R-P), and (c) Temkin isotherm models.

Table 4. Isotherm constants for adsorption of nickel (II) ions onto alginate-SBA-15 nanocomposite.

Isotherm	Parameters			
Langmuir Eq.	q_{max} (mg g^{-1})	K_l (L $mmol^{-1}$)		R^2
	58.82	1.717		0.999
Freundlich Eq.	n	K_f (mg g^{-1} mM^{-1})		R^2
	0.5408	55.69		0.965
R-P Eq.	K_R	α_R	β_R	R^2
	70.14	1	1	0.9531
D-R Eq.	β_D	q_m (mg g^{-1})		R^2
	1E-7	52.92		0.9837
Temkin Eq.	A_T	K_T		R^2
	0.005	20.27		0.9869

Comparison of alginate-SBA-15 adsorbent performance with literature data

A comparatative study on adsorbent performance for nickel removal from aqueous solution with different adsorbents reported in the literature [21-24] is listed in Table 5. Comparison of q_{max} values revealed that the alginate-SBA-15 nanocomposite has great ability in the adsorption of nickel (II) ions than others; however, their surface was improved by functionalization. Both the electronegative cavities and the functional groups (i.e carboxyl and oxygen-containing groups) on the highest adsorption performance of the alginate-SBA-15 nanocomposite take part. Intrinsically, the nanoporous adsorbents such as SBA-15 caused some difficulties during separation process due to their ultrafine structures. The improved physical structure and high mechanical stability of the alginate-SBA-15 nanocomposite overcome these limitations.

Table 5. Comparison of the alginate-SBA-15 adsorption capacity in this study with previously related researches for nickel (II) ions removal.

Adsorbate	q_{max} (mg g^{-1})	Ref.
SBA-15(SH) [a]	0.51	[21]
SBA-15 [b]	1.02	[21]
SBA-15 [c]	8.3	[22]
SBA-15 [e]	22	[22]
SBA-15 [f]	11.7	[23]
MCM-41 (pore expanded)	54.47	[24]
Alginate-SBA-15	58.82	This work

[a]Thiol-functionalized SBA-15, [b]Amino-functionalized SBA-15, [c]N-Propylsalicylaldimino-functionalized SBA-15, [e]Salicylaldehyde functionalized SBA-15, [f]EDTA modified G3-PAMAM-SBA-15.

Conclusion

In this study, a biopolymer adsorbent was developed using mesoporous silica SBA-15 and calcium alginate by encapsulation method. This method modified the ultrafine structure of SBA-15 and improved it for practical purposes. The present work also demonstrates sorption performance of alginate-SBA-15 nanocomposite in the removal of nickel (II) from aqueous solution. Through the adsorption experiment, it observed that adsorption of nickel onto alginate-SBA-15 strongly occur at pH 2 to 7. The resultsof kinetic study revealed that the sorption kinetics is fast and obey from pseudo-second-order model as shown by its correlation coefficient. Also, out of several isotherm models, the Langmuir, Ferundlich, Dubinin-Radushkevich, Redlich-Peterson, and Temkin models are applied to experimental data. The Langmuir isotherm model was found to be fitted well to the isotherm equilibrium data than the other equations, indicating homogenous surface with identical binding sites for alginate-SBA-15 nanocomposite. The maximum adsorption capacity (qmax) of the alginate-SBA-15 nanocomposite was calculated as 58.82 mg g^{-1}.

References

[1] V. Kinhikar, *Res. J. Chem. Sci*., 2, 6 (2012).

[2] Z. Aksu, *Process Biochem*., 38, 89 (2002).

[3] Y. Vijaya, S.R. Popuri, V.M. Boddu , A. Krishnaiah, *Carbohydr. Polym*., 72, 261 (2008).

[4] U. K. Garg, M. Kaur, V. Garg, D. Sud, *Bioresour.Technol*., 99, 1325 (2008).

[5] V. Srivastava, C. Weng, V. Singh , Y. Sharma, *J. Chem. Eng. Data*, 56, 1414 (2011).

[6] Y. Ho, D.J. Wase, C. Forster, *Water Res.,* 29, 1327 (1995).

[7] N.R. Axtell, S.P. Sternberg , K. Claussen, *Bioresour.Technol*., 89, 41 (2003).

[8] K. Vijayaraghavan, J. Jegan, K. Palanivelu , M. Velan, *J.Hazard.Mater*., 113, 223 (2004).

[9] M. I. Kandah , J.L. Meunier, *J.Hazard. Mater*., 146, 283 (2007).

[10] A. Navarro, H. Musaev, K. Serrano, M. Masud, *J. Earth. Sci. Clim. Change*, 5, 2 (2014).

[11] R. Karthik, S. Meenakshi, *Int.J.Biol. Macromol*., 72, 711 (2015).

[12] J.H. Chen, H.T. Xing, H.X. Guo, G.P. Li, W. Weng , S.R. Hu, *J.Hazard.Mater*., 248, 285 (2013).

[13] R. Cheraghali, H. Tavakoli , H. Sepehrian, *Scientia Iranica*, 20, 1028 (2013).

[14] A.A. Attia, S.A. Khedr , S.A. Elkholy, *Brazilian J. Chem. Eng*., 27, 183 (2010).

[15] M. Makeswari, T. Santhi, *Arabian J. Chem*., (2014).

[16] S.H. Asl, M. Ahmadi, M. Ghiasvand, A. Tardast , R. Katal, *J. Ind. Eng. Chem*., 19, 1044 (2013).

[17] Y. Ho, J. Porter, G. McKay, *Water, Air, and Soil Pollut*., 141, 1 (2002).

[18] C. Gok , S. Aytas, *J.Hazard.Mater*., 168,

369 (2009).

[19] T.A. Davis, B. Volesky , A. Mucci, *Water Res*., 37, 4311 (2003).

[20] K. Sing, *Colloids Surf., A*, 187, 3 (2001).

[21] A. Liu, K. Hidajat, S. Kawi , D. Zhao, *Chem. Commun*., 1145 (2000).

[22] M. Mureseanu, A. Reiss, I. Stefanescu, E. David, V. Parvulescu, G. Renard, V. Hulea, *Chemosphere*, 73, 1499 (2008).

[23] Y. Jiang, Q. Gao, H. Yu, Y. Chen, F. Deng, *Micropor. Mesopor. Mater*., 103, 316 (2007).

[24] A. Sayari, S. Hamoudi, Y. Yang, *Chem. Mater*., 17, 212 (2005).